A High Efficiency, Decoupled On-board Battery Charger with Magnetic Control

Yuqi Wei[1,2], Necmi Altin[1,3], Quanming Luo[2], Adel Nasiri[1]
[1]Department of Electrical Engineering, University of Wisconsin-Milwaukee, Milwaukee, Wisconsin, USA
[2]Department of Electrical Engineering, Chongqing University, Chongqing, China
[3]Department of Electrical and Electronic Engineering, Faculty of Technology, Gazi University, Ankara, Turkey
Email: yuqiwei@uwm.edu; altin@uwm.edu; lqm394@126.com; nasiri@uwm.edu

***Abstract*—In this paper, a high efficiency, decoupled on-board battery charger is proposed. The proposed topology is composed of two LLC resonant converters sharing the same full-bridge inverter with constant switching frequency. The outputs of two LLC resonant converters are connected in series. One of the LLC resonant converters is operated at the resonant frequency, which is the highest efficiency operation point. The magnetic control is adopted for the second LLC resonant converter to fulfill the closed-loop control of charge voltage and current for constant voltage (CV) and constant current (CC) charge modes. The proposed topology can achieve zero voltage switching (ZVS) for all primary switches and zero current switching (ZCS) for all secondary diodes during both CC and CV modes. Furthermore, thanks to constant frequency operation, the electromagnetic interference (EMI) filter design is simplified. Simulation and experimental studies are presented to verify the feasibility and validity of the proposed topology.**

Keywords—High efficiency; LLC resonant converter; decoupled; magnetic control; battery charger;

I. Introduction

Nowadays, there is a growing interest in electric vehicles (EV) and plug-in hybrid electric vehicles (PHEV) due to their environmental-friendly characteristics [1]-[3]. This has also increased the attention on battery charger technologies. Many topologies for battery charger have been proposed [4]-[9]. Among these topologies, LLC resonant converter has been widely adopted for the battery charger application due to the soft-switching capability [10]-[15]. The frequency control, phase shift control or modified structures are applied to LLC resonant converters to obtain constant current (CC) and constant voltage (CV) charge modes. The frequency control [10], [11] is a common control technique used in LLC resonant converters. However, due to wide range of output voltage, a large variable frequency range is required for battery charger applications, which makes the design of magnetic components and EMI filter complicated. Although the phase shift control [12], [13] limits the required switching frequency, the soft switching capability is a tricky problem and it is not suitable for heavy load operation. The modified control structures [14] require additional switches. Since these additional switches are hard switching, they lead to lower efficiency. In [15], a novel topology with two LLC resonant converters sharing the same full-bridge inverter is proposed. This topology requires an additional switch and capacitor, which make the system more complex.

In this study, two LLC resonant converters sharing the same full-bridge inverter operating at the resonant frequency is proposed. The proposed topology is shown in Fig. 1. The outputs of the LLC converters are connected in series. The magnetic control is adopted to control the CV and CC charge modes. Thus, phase shift requirement in [12], [14] and additional switch requirement in [15] is removed. In addition, the system control is simplified due to the capability of adjusting the variable inductor continuously. Since the switching frequency is constant and close to the resonant frequency, the proposed converter operates at its highest efficiency operation point. The decoupling idea is adopted to further improve system efficiency.

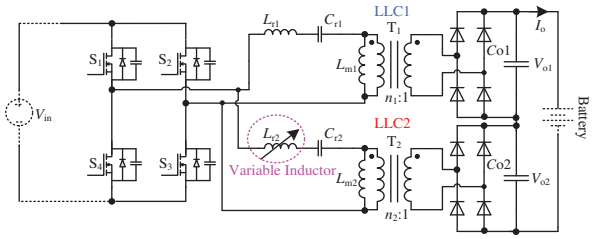

Fig. 1. The proposed topology for battery charger.

This paper is organized as follows: system operation analysis is given in Section II; in Section III, the magnetic control is introduced; design considerations are presented in Section IV; simulation and experimental studies are analyzed in Section V and finally, a conclusion is drawn.

II. Operation Analysis

There are two resonant frequencies in an LLC resonant converter. These frequencies can be expressed as follows:

$$f_r = \frac{1}{2\pi\sqrt{L_r C_r}} \tag{1}$$

$$f_m = \frac{1}{2\pi\sqrt{(L_r + L_m) C_r}} \tag{2}$$

978-1-5386-5982-3/18/$31.00 ©2018 IEEE

According to fundamental harmonic analysis (FHA), the AC equivalent model of an LLC resonant converter can be obtained as shown in Fig. 2, where R_{ac} is the equivalent resistance of the rectifier network, and it can be expressed as

$$R_{ac} = \frac{8n^2}{\pi^2} R_L \tag{3}$$

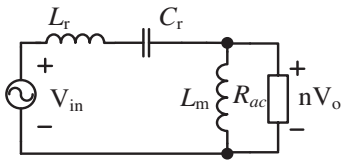

Fig. 2. AC equivalent model of an LLC resonnat converter.

The output voltage can be obtained according to voltage divider law.

$$V_o(s) = n \frac{V_{in}}{1 + \dfrac{L_r s + \dfrac{1}{C_r s}}{L_m s} + \dfrac{1}{R_{ac}}\left(L_r s + \dfrac{1}{C_r s}\right)} \tag{4}$$

The output current can be derived by dividing the equivalent resistance R_{ac}.

$$I_o(s) = \frac{V_o(s)}{R_{ac}} = \frac{1}{n} \frac{V_{in}}{R_{ac}\left(1 + \dfrac{L_r s + \dfrac{1}{C_r s}}{L_m s}\right) + L_r s + \dfrac{1}{C_r s}} \tag{5}$$

These two resonant frequencies correspond to two basic characteristics of LLC resonant converter. When the switching frequency equals to the resonant frequency f_r, it is seen from the output voltage equation (4) that the term associated with the load becomes zero, which means the output voltage is independent from the load. When the switching frequency equals to second resonant frequency f_m, as seen from the output current equation (5), the term associated with the load becomes zero, so the output current is constant and independent from the load.

For the proposed topology, LLC1 is always operating at the constant output voltage mode, which can be considered as a voltage source. The operation mode of LLC2 can be changed from constant output current to constant output voltage mode to fulfill the CC charge and CV charge requirement of the battery. This principle can be summarized as: 1) when both LLC resonant converters are operating at constant output voltage mode, the output voltage is constant; 2) when LLC1 is operating at constant output voltage mode and LLC2 is operating at constant output current mode, the output current is constant. In addition, since LLC1 is operating at the highest efficiency operation point during the whole operation and the LLC2 is used to achieve closed-loop control with a variable resonant frequency range, thanks to the magnetic control, the overall system efficiency is improved comparing with conventional single LLC resonant converter topology. Furthermore, low rated components can be selected to further improve efficiency due to series connection of the outputs.

III. Magnetic Control

In the proposed topology, the magnetic control (variable inductor) is adopted. By using variable inductor, a constant switching frequency operation is achieved, which simplifies both the EMI filter and control circuit design. In addition, the variable inductor has been applied in many applications [16], [17], like LED drivers, dimming of fluorescent lamps, voltage control in resonant converters.

The structure of the variable inductor using a double E-core shown in Fig. 3. The control winding or auxiliary winding is divided into two identical portions with the number of turns N_{DC}, which is mounted on the lateral legs of the core. The inductor winding or main winding with the number of turns N_{AC} is placed on the air-gapped middle leg of the core. The DC bias current allows the modification of the inductance of the main winding.

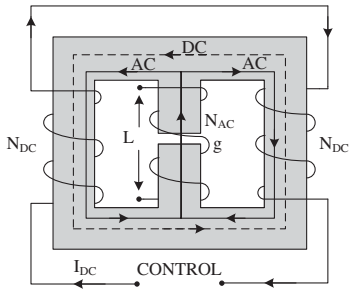

Fig. 3. Structure of the variable inductor.

The control scheme is shown in Fig. 4, the error is obtained by comparing the reference voltage/current and the feedback voltage/current, and then applied to the PI controller. The PI controller generates the control signal which is used to adjust the DC bias current which controls the inductance value of the variable inductor. Thus, the inductance value can be adjusted to regulate the output voltage.

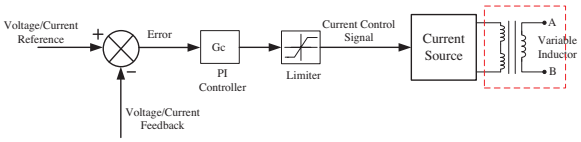

Fig. 4. Control Scheme of the system.

IV. Design Considerations

The decoupling idea of the proposed topology is shown in Fig. 5. For a battery, the CC charge stage gets most of the output power, and in the proposed structure, the role of LLC1 is to handle as much power as possible because it is working at the highest efficiency operation point, while the role of LLC2 is to provide close loop control to regulate the output voltage

and current of the system. The power handled by LLC2 ranges from 9% to 40% in this research. Therefore, the system efficiency can be further improved.

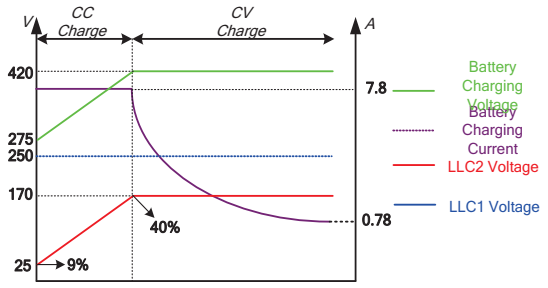

Fig. 5. Battery charging profile of the proposed topology.

The design guideline for the system is summarized as follows: First, the resonant inductance value in CC and CV modes which gives the range of variable inductor should be found for LLC2; then, the resonant network of the LLC1 is designed to make sure the total input impedance is inductive, so ZVS operation for the primary switches is achieved. The detailed design procedures are given in next subsections.

A. Selection of transformers turns ratio

The known parameters of the system are input voltage and switching frequency: V_{in}=400V, f_s=200kHz. Since two LLC resonant converters are both working at constant output voltage mode in CV mode, their voltage gain are unity. Based on this characteristic, the turns ratio of T1 and T2 can be obtained.

$$n_1 = \frac{V_{in}}{V_{o1}} = \frac{400}{250} = 1.6 \tag{6}$$

$$n_2 = \frac{V_{in}}{V_{o2}} = \frac{400}{170} = 2.35 \tag{7}$$

B. Selection of resonant components of LLC2

According to above analysis, LLC2 is working at the constant output current mode during CC charge. Based on (5), the expression of magnetic inductor L_{m2} can be obtained as follows:

$$L_{m2} = \frac{n_2 V_{in}}{I_o 2\pi f_s} = \frac{2.35\times 400}{7.8\times 2\times 3.14\times 200\times 10^3} = 96uH \tag{8}$$

The design guideline for resonant inductor L_{r2} is the RMS current of the resonant tank, which is related to the losses. The RMS current can be expressed as in (9):

$$I_{Lr2,RMS} = \sqrt{\sum_{N=1,3,5\cdots}^{\infty} \left(\frac{4V_{in}}{\sqrt{2}N\pi \left|Z_{in2}(jNw_s)\right|}\right)^2} \tag{9}$$

where w_s is the angular frequency, and Z_{in2} is the input impedance of LLC2. They can be expressed as in (10) and (11) respectively.

$$w_s = 2\pi f_s \tag{10}$$

$$Z_{in2}(jNw_s) = L_{r2}jNw_s + \frac{1}{C_{r2}jNw_s} + \frac{L_{m2}jNw_s R_{ac2}}{L_{m2}jNw_s + R_{ac2}} \tag{11}$$

Based on the battery charging profile, the range of equivalent resistance R_{ac2} during CC mode can be found as given below:

$$R_{ac2,\min,CC} = \frac{8n_2^2}{\pi^2}\cdot R_{L2,\min,CC} = \frac{8\times 2.35^2}{3.14^2}\times\frac{25}{7.8} = 14.35\Omega \tag{12}$$

$$R_{ac2,\max,CC} = \frac{8n_2^2}{\pi^2}\cdot R_{L2,\max,CC} = \frac{8\times 2.35^2}{3.14^2}\times\frac{170}{7.8} = 97.56\Omega \tag{13}$$

Since C_{r2} is dependent on L_{r2} according to (2), combining equations (2), (9)-(13), the RMS current of the resonant tank with different resonant inductor value can be plotted by using MATLAB as shown in Fig. 6, where the blue line represents the maximum equivalent resistance, and the red line represents the minimum equivalent resistance.

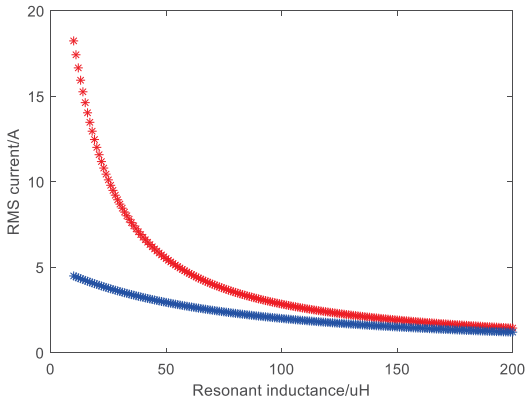

Fig. 6. RMS current of the resonant tank with different resonant inductance value.

From Fig. 6, by taking losses and inductor size into consideration, a reasonable resonant inductance value L_{r2} equals 40uH is selected. Since the constant frequency operation is implemented, the resonant inductance in CV mode can be calculated as in (14):

$$L_{r2,CV} = L_{r2,CC} + L_{m2} = 136uH \tag{14}$$

According to (1), the resonant capacitor C_{r2} can be calculated:

$$C_{r2} = \frac{1}{4\pi^2 f_s^2 L_{r2,CV}} = 4.66nF \ . \quad (15)$$

C. Selection of resonant components of LLC1

As mentioned before, the design guideline for LLC1 is to make sure the total input impedance of the system is inductive, so the primary switches can achieve ZVS operation. Due to the parallel connection of their inputs, the total input impedance can be expressed as in (16):

$$Z_{in} = Z_{in1} // Z_{in2} \ . \quad (16)$$

Since LLC1 is always operating at resonant frequency f_r, its input impedance can be simplified as follows:

$$Z_{in1} = \frac{L_{m1} s R_{ac1}}{L_{m1} s + R_{ac1}} \quad (17)$$

where R_{ac1} can be expressed as

$$R_{ac1,CC} = \frac{8n^2}{\pi^2} \cdot R_{Ld1,CC} = 66.51\Omega \ . \quad (18)$$

The worst condition is considered, so the minimum value of R_{ac1} is used in analyze. Figure. 7 shows the total input impedance angle with different value of L_{r2} and L_{m1}, where the red line represents the results for L_{m1} equals 10uH, the blue line is for L_{m1} equals 20uH and the green line is for L_{m1} equals 30uH. It can be seen that magnetic inductance no greater than 20uH is required in order to achieve ZVS operation for all operation conditions. However, the magnetic inductance value is related to RMS current of the resonant tank, by taking both into consideration, a magnetic inductance value equals 20uH is selected.

For the resonant inductor L_{r1} and resonant capacitor C_{r1}, the design guideline is the voltage stress on the resonant capacitor. According to (1), the resonant capacitor value is inversely proportional with the resonant inductor value; in addition, the voltage stress on the resonant capacitor is also inversely proportional with its value. Therefore, a lower resonant inductor value and a higher resonant capacitor value is preferred. Finally, L_{r1} equals 10uH and C_{r2} equals 63.3nF are selected.

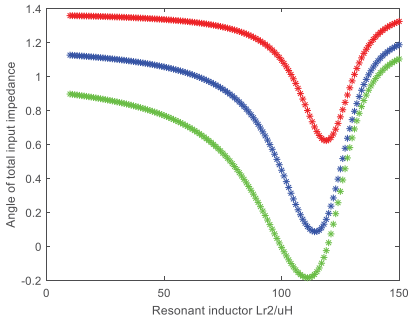

Fig. 7. Input impedance angle with different value of Lr2 and Lm1.

V. Simulation and Experimental Results

In this part, the variable inductor is implemented, and the simulation and experimental results are compared and analyzed. Then, a simulation case is introduced to verify the operation of the proposed topology.

According to the requirements, EE42 core with PC40 material is selected to implement variable inductor. The physical structure is shown in Fig. 8.

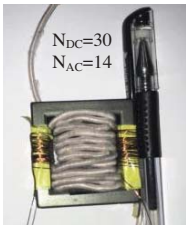

Fig. 8. Physical structure of implemente variable inductor.

The test system for variable inductor is shown in Fig. 9, which is composed of a LCR meter, a power supply and the variable inductor. The initial value of the variable inductor is 172.71uH.

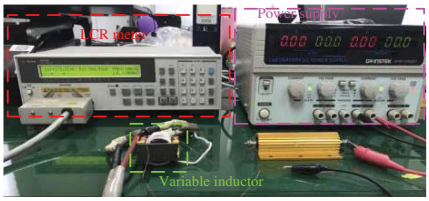

Fig. 9. Test system for variable inductor.

According to the SPICE modeling method proposed in [17], the variable inductor designed in this paper is modeled and simulated in LTspice. The simulation results and experimental results are compared in Fig. 10. It can be seen that the simulation results agree with the experimental results. Therefore, the model can provide an effective guideline when designing a variable inductor.

Then, the operation of the proposed topology is verified in PSIM, and the simulation results are presented. Five operation points from the battery charging profile shown in Fig. 11 are selected to verify theoretical analysis.

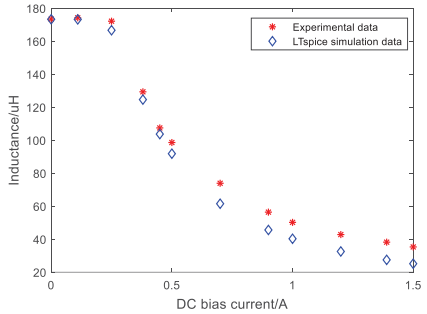

Fig. 10. Comparasion between simulation and experiment.

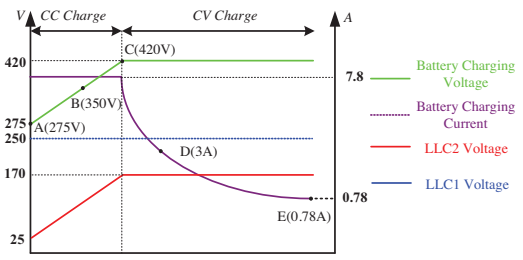

Fig. 11. Five operation points selected from the battery charging profile.

Figure. 12 shows the simulation results of operation point A, which is also the beginning point of CC charge, including output voltages of two LLC resonant converters, output current and total resonant current and resonant voltage. Similarly, Figure. 13-16 show the simulation results of operation point B, C, D, E, respectively.

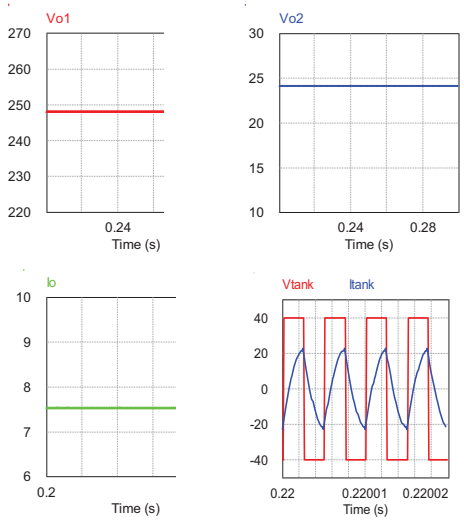

Fig. 12. Simulation results of operation point A.

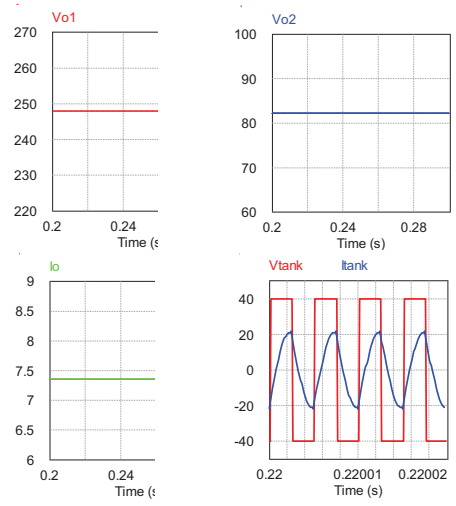

Fig. 13. Simulation results of operation point B.

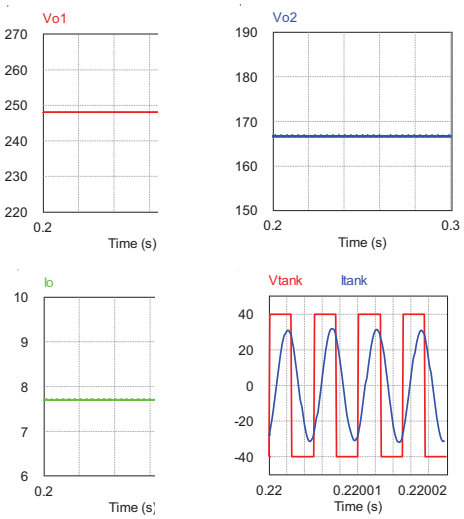

Fig. 14. Simulation results of operation point C.

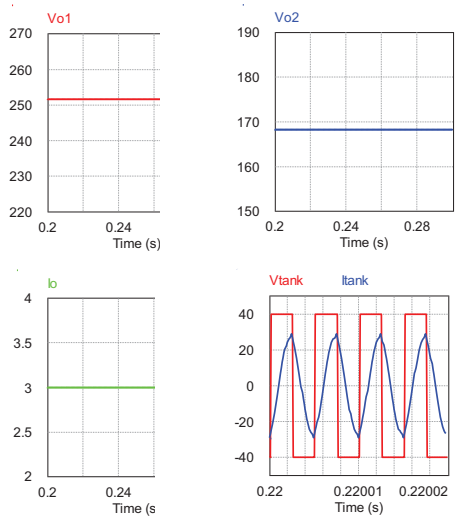

Fig. 15. Simulation results of operation point D.

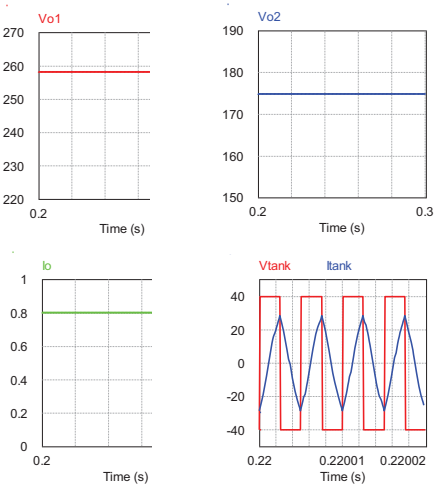

Fig. 16. Simulation results of operation point E.

According to the simulation results, the output voltage of LLC1 is almost remain constant at 250V. For LLC2, the output voltage increases from about 25V to 170V during CC charge, and remain constant at 170V during CV charge. In addition, the total resonant current lags behind the resonant voltage during whole operation range, which means the ZVS operation can be achieved for the primary switches. Since the switching frequency is always equal or lower than the resonant frequency for LLC converters, the ZCS operation for the rectifier diodes can be guaranteed. Based on the five operation points, the output voltage characteristic of two LLC resonant converters can be drawn.

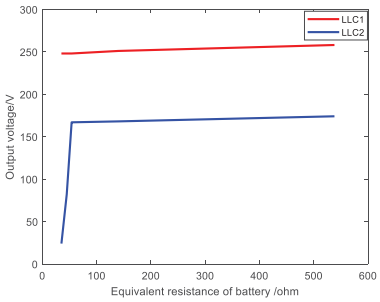

Fig. 17. Output voltage of two LLC resonant converter.

VI. Conclusion

In this study, two LLC resonant converters sharing the same full-bridge inverter operating at the resonant frequency is proposed. The magnetic control is adopted to control the charge modes. The advantages of the proposed battery charger topology are summarized as follows: 1) high power handing ability due to parallel connection of two LLC resonant converters; 2) system efficiency is improved by adopting the decoupling idea and the magnetic control; 3) EMI design is simplified by implementing a constant frequency, and no phase shift is required for the primary switches; 4) ZVS operation for the primary switches and ZCS operation for the secondary diodes are achieved by carefully designing resonant tanks. The experimental validation will be the focus of the future work.

Acknowledgment

This research was supported by the National Nature Science Foundation of China under Grant 51577019, China Scholarship Council (CSC). Dr. Necmi Altin thanks financial support from the Scientific and Technological Research Council of Turkey (TUBİTAK) BIDEB-2219 Postdoctoral Research program.

References

[1] Z. Cerovsky, P. Mindl, “Impact of energy production technology on gas emission by electric hybrid and electric vehicles”, International Journal of Renewable Energy Research (IJRER), vol. 1, no. 3, pp. 118-125, 2011.

[2] A. Elgammal, A. M. Sharaf, “A hybrid pv-fc-diesel-battery efficient schemes for four-wheel PMDC electric vehicle drive system”, International Journal of Renewable Energy Research (IJRER), vol. 2, no. 1, pp. 53-77, 2012.

[3] T. Harighi, R. Bayindir, E. Hossain, “Overview of quality of service evaluation of a charging station for electric vehicle”, 2017 IEEE 6th International Conference on Renewable Energy Research and Applications (ICRERA), 2017, pp. 1180-1185.

[4] Vi. M. Iyer, S. Gulur, Su. Bhattacharya, “Variable DC bus control for a bidirectional on-board electric vehicle charger”, 2017 IEEE 6th International Conference on Renewable Energy Research and Applications (ICRERA), 2017, pp. 1041-1046.

[5] V. Castiglia, L. Di Noia, P. Livreri, R. Miceli, C. Nevoloso , F. Pellitteri, F. Viola, “An efficient wireless power transfer prototype for electrical vehicles”, 2017 IEEE 6th International Conference on Renewable Energy Research and Applications (ICRERA), 2017, pp. 1215-1220.

[6] B. Khaki, A. M. Sharaf, “A hybrid multi-loop controlled facts-based smart V2G battery chargers”, International Journal of Renewable Energy Research (IJRER), vol. 3, no. 1, pp. 155-160, 2013.

[7] S. Hattori, H. Eto, F. Kurokawa, “High power density battery charger for plug-in micro EV”, International Journal of Renewable Energy Research (IJRER), vol. 8, no. 2, pp. 1006-1015, 2018.

[8] E. Şanal, P. Dost, C. Sourkounis, “LCL-Filter design for a battery charger based on buck converter (DCDC converter)”, 2016 IEEE International Conference on Renewable Energy Research and Applications (ICRERA), 2017, pp. 617-621.

[9] K. Colak, E. Asa, D. Czarkowski, “Dual closed loop control of LLC resonant converter for EV battery charger”, 2013 IEEE International Conference on Renewable Energy Research and Applications (ICRERA), 2013, pp. 811-815.

[10] H.-P. Park, J.-H. Jung, “Modeling and feedback control of LLC resonant converters at high switching frequency”, Journal of Power Electronics, Vol. 16, No. 3, pp. 849-860, 2016.

[11] Z. Hu, Y. Qiu, Y.-F. Liu, P. C. Sen “A control strategy and design method for interleaved llc converters operating at variable switching frequency”, IEEE Transactions on Power Electronics, Vol. 29, No. 8, pp. 4426-4437, 2014.

[12] J.-H. Kim, C.-E. Kim, J.-K. Kim, J.-B. Lee, G.-W. Moon, “Analysis on load-adaptive phase-shift control for high efficiency full-bridge LLC resonant converter under light-load conditions”, IEEE Transactions on Power Electronics, Vol. 31, No.7, pp. 4942-4955, 2016.

[13] K. Zheng, D. Zhou, J. Li, L. Li, Y. Zhao, “A Digital self-sustained phase shift modulation control strategy for full-bridge LLC resonant converters”, Journal of Power Electronics, Vol. 16, No.3, pp. 915-924, 2016.

[14] H. Hu, X. Fang, F. Chen, Z. J. Shen, I. Batarseh “A modified high-efficiency LLC converter with two transformers for wide input-voltage range applications”, IEEE Transactions on Power Electronics, Vol. 28, No.4, pp. 1946-1960, 2013.

[15] Vu H N, Choi W J, “A novel dual full-bridge LLC resonant converter for cc and cv charges of batteries for electric vehicles”, IEEE Transactions on Industrial Electronics, Vol. 65, No.3, pp. 2212-2225, 2017.

[16] Alonso J M, G. Martínez, M. Perdigão, M. R. Cosetin, R. N. do Prado, “A systematic approach to modeling complex magnetic devices using SPICE: application to variable inductors”. IEEE Trans. Power Electron., Vol. 31, No. 11, pp. 7735-7746, 2016.

[17] J. M. Alonso, M. Perdigao, G. Z. Abdelmessih, M. A. Dalla Costa, Y. Wang, “SPICE modeling of variable inductors and its application to single inductor LED driver design” IEEE Transactions on Industrial Electronics., No. 99, pp.5894-5903, 2016.